

Tropospheric Delay Calibration System Performance During the First Two BepiColombo Solar Conjunctions

Riccardo Lasagni Manghi¹ , David Bernacchia¹ , Luis Gomez Casajus² , Marco Zannoni^{1,2} , Paolo Tortora^{1,2} , Antonio Martellucci³, Javier De Vicente⁴, Jose Villalvilla⁴ , Gerrit Maschwitz⁵ , Paolo Cappuccio⁶ , and Luciano Iess⁶ 

¹Dipartimento di Ingegneria Industriale, Alma Mater Studiorum - Università di Bologna, Forlì, Italy, ²Centro Interdipartimentale di Ricerca Industriale Aerospaziale, Alma Mater Studiorum - Università di Bologna, Forlì, Italy, ³European Space Agency, ESA-ESTEC, Noordwijk, The Netherlands, ⁴European Space Agency, ESA-ESOC, Darmstadt, Germany, ⁵RPG Radiometer Physics GmbH, Meckenheim, Germany, ⁶Department of Mechanical and Aerospace Engineering, Sapienza University of Rome, Rome, Italy

Key Points:

- The Tropospheric Delay Calibration System installed at the Malargüe ground station was operated during the BepiColombo solar conjunctions
- The system calibrations improved the Doppler measurements by 51% on average and up to 73% in optimal conditions
- Calibrated two-way Doppler residuals satisfy the Mercury Orbiter Radioscience Experiment stability requirements

Correspondence to:

R. Lasagni Manghi,
riccardo.lasagni@unibo.it

Citation:

Lasagni Manghi, R., Bernacchia, D., Gomez Casajus, L., Zannoni, M., Tortora, P., Martellucci, A., et al. (2023). Tropospheric delay calibration system performance during the first two BepiColombo solar conjunctions. *Radio Science*, 58, e2022RS007614. <https://doi.org/10.1029/2022RS007614>

Received 11 OCT 2022
Accepted 22 JAN 2023

Author Contributions:

Conceptualization: Riccardo Lasagni Manghi, Marco Zannoni, Gerrit Maschwitz, Luciano Iess
Data curation: Riccardo Lasagni Manghi, David Bernacchia, Luis Gomez Casajus, Marco Zannoni, Javier De Vicente, Jose Villalvilla
Formal analysis: Riccardo Lasagni Manghi
Funding acquisition: Antonio Martellucci
Investigation: Javier De Vicente, Jose Villalvilla
Methodology: Gerrit Maschwitz
Project Administration: Paolo Tortora, Antonio Martellucci
Resources: Paolo Tortora

Abstract Media propagation delay and delay-rate induced by the water vapor within the Earth's troposphere represent one of the main error sources for radiometric measurements in deep space. In preparation for the BepiColombo and JUICE missions, the European Space Agency has installed and operates the prototype of a tropospheric delay calibration system (TDCS) at the DSA-3 ground station located in Malargüe, Argentina. An initial characterization of the TDCS performance was realized using two-way Doppler measurements at X-band to perform the orbit determination of the Gaia spacecraft. This work will further characterize the system by analyzing two-way Doppler and range data at X- and Ka-band for 31 tracking passes of the BepiColombo spacecraft, which were recorded between March 2021 and February 2022 during the first two solar conjunction experiments. The performance exceeds the expectations based on the previous analysis, with a reduction of the Doppler noise of 51% on average and up to 73% when using the TDCS measurements in place of standard calibrations based on global navigation satellite system data. Furthermore, the campaign serves as validation of the TDCS operations during superior solar conjunctions, with most of the tracking passes at low elongation now satisfying the Mercury orbiter radioscience experiment requirements on two-way Doppler stability. These results, which are in line with those of similar instruments installed at other Deep Space Network antennas, are obtained using a commercial microwave radiometer with significantly lower installation and maintenance costs.

1. Introduction

Radioscience experiments in recent deep space missions like Cassini, Juno, and BepiColombo, have reached very high standards in terms of accuracy and reliability thanks to the very precise radio tracking systems installed on the probes and on the ground. This high level of precision can be reached through the combination of X- and Ka-band communication links for both uplink and downlink, thanks to the simultaneous usage of two on-board transponders (Bertotti et al., 1993; Iess et al., 2009; Serra et al., 2019). The linear combination of radiometric observables obtained through multi-frequency links allows to remove dispersive media propagation errors caused by the solar and interplanetary plasma and the Earth's ionosphere, which represent two of the largest noise sources in radio tracking. This improvement in radio systems' technology consequently led to increasingly demanding requirements in order to obtain higher accuracy during the orbit determination process.

For instance, the Mercury orbiter radioscience experiment (MORE) onboard BepiColombo, which will perform analyses in gravity science, geodesy and fundamental physics (Iess et al., 2021), has a Doppler stability requirement, expressed in terms of Allan deviation, of $1.4 \cdot 10^{-14}$ for time intervals larger than 1,000 s, corresponding to an accuracy in range rate of about 0.004 mm/s (di Stefano et al., 2021). At the same time, the availability of an onboard Ka-band transponder (KaT) enables precise pseudo-noise ranging measurements that have proven to reach an accuracy of less than 1 cm during tests performed on inflight data (Cappuccio et al., 2020).

As a consequence, the focus has recently shifted towards the removal of non-dispersive error sources such as the ones due to the ground station hardware or the Earth's troposphere, which represent the highest noise contributors after the plasma-noise removal (Iess et al., 2012).

© 2023. The Authors.

This is an open access article under the terms of the [Creative Commons Attribution License](https://creativecommons.org/licenses/by/4.0/), which permits use, distribution and reproduction in any medium, provided the original work is properly cited.

Software: Riccardo Lasagni Manghi, David Bernacchia, Luis Gomez Casajus, Marco Zannoni, Gerrit Maschwitz

Supervision: Marco Zannoni, Paolo Tortora, Antonio Martellucci, Luciano Iess

Validation: Paolo Cappuccio

Visualization: Riccardo Lasagni Manghi, David Bernacchia, Luis Gomez Casajus

Writing – original draft: Riccardo Lasagni Manghi, David Bernacchia

Writing – review & editing: Paolo Tortora, Antonio Martellucci, Jose Villalvilla, Gerrit Maschwitz, Paolo Cappuccio, Luciano Iess

In preparation for the BepiColombo and Juice missions, the European Space Agency has installed and operates the prototype of a new Tropospheric Delay Calibration System (TDCS) at the DSA-3 deep space ground station in Malargüe. This system, which is based on a high stability microwave radiometer, uses a combination of sky brightness temperature measurements at Ka- and V-bands to retrieve the path delay induced by water vapor along the instrument's line of sight. The artificial neural network used to retrieve the path delay was specifically trained for the Malargüe site using a large set of atmospheric vertical profiles from the ERA-Interim reanalysis database of the European Center for Medium Weather Forecast (ECMWF).

An initial system qualification test has been carried out using the TDCS calibrations for the orbit determination of the Gaia spacecraft, by analyzing the statistics of Doppler residuals for 32 tracking passes. The analysis has shown that using TDCS data in place of standard calibrations can significantly improve the quality of the Doppler measurements, with an average noise reduction of 34% and up to 61% (Lasagni Manghi et al., 2021).

However, the applicability of the Gaia orbit determination results is limited by the geometrical and operational conditions which characterize its tracking passes. Specifically, Gaia operates near solar opposition, which means that all tracking passes occur at night when the water vapor content and turbulent mixing in the troposphere are minimized. Furthermore, Gaia uses a single-frequency communication link at X-band, which is affected by dispersive noise sources such as the charged particles in the Earth's ionosphere (the effect of solar plasma is marginal given the high elongation angles).

In this work, we further characterize the TDCS performance by analyzing the BepiColombo tracking passes that were recorded during the cruise phase as part of the first two solar conjunction experiments (SCE). The availability of a multi-frequency link at X- and Ka-bands for both Doppler and range measurements makes the BepiColombo mission a perfect testbed for addressing the contribution of tropospheric calibrations to the overall data quality, due to the cancellation of the dispersive noise sources. More severe tropospheric conditions, in terms of water vapor content and variability, are also expected for the BepiColombo tracking passes, which occur during the daytime. Finally, this campaign represents the first operational test of the TDCS during superior solar conjunction and should validate the so called *Sun avoidance* strategy for observations at Sun-Earth-probe (SEP) angles below 3°.

In the following sections, 31 tracking passes recorded at the Malargüe ground station between March 2021 and February 2022 are analyzed as part of an orbit determination process. The noise characteristics of the range and Doppler measurement residuals obtained using the TDCS calibrations are compared to those obtained using standard tropospheric calibrations based on global navigation satellite system (GNSS) data. Finally, the noise characteristics are compared with the MORE requirements to verify the end-to-end system compliance.

2. Tropospheric Delay Calibration System

The TDCS is a prototype instrument for the estimation of the tropospheric delay and delay-rate along the line of sight of a deep space antenna. Its main subsystem is represented by a high-stability microwave radiometer, which measures the sky noise emissions at 14 frequency channels near the water vapor absorption line at 22.4 GHz, the oxygen absorption band around 60 GHz, and in the 30 GHz window that is mainly sensitive to liquid water content.

This prototype includes a modified version of the HATPRO-G5 model developed by Radiometer physics GmbH, an external parabolic reflector to reduce the antenna beam width, an open-loop antenna control system for tracking passes of deep space missions, and a meteorological station. The TDCS includes a dew blower/heater system to remove water condensation from the exposed surfaces of the antenna system. It is completed by new calibration and tracking procedures, and software tools specifically developed for monitoring, automatic control, and commanding by the ground station systems. More details on the system are provided by Lasagni Manghi et al. (2021) that used a similar setup for the orbit determination of the Gaia spacecraft.

3. Testbed Summary and Data Availability

Table 1 provides an overview of the 31 BepiColombo tracking passes that were analyzed during this study and of the atmospheric conditions which were encountered during each pass. The first 17 passes are related to the first solar conjunction experiment (SCE1), which occurred between 10 and 26 March 2021, corresponding to the local

Table 1

Summary of Data Availability and Main Meteorological Parameters for the Analyzed Tracking Passes

Year	DOY	Date	From/to	Elevation (°)	LWP (g/m ²)	ZWD (mm)	WS (km/hr)	RR (mm/hr)	RR _{pass} (mm/hr)	Pointing offset (°)
2021	69	10 March	(12:45, 21:00)	(31, 61, 23)	56	(36, 58)	48	–	–	–
	70	11 March	(12:37, 20:50)	(28, 60, 25)	39	(60, 86)	26	–	–	–
	71	12 March	(12:38, 21:00)	(28, 60, 23)	54	(93, 135)	16	–	–	–
	72	13 March	(12:50, 21:00) ^a	(29, 59, 23)	6,722	(89, 209)	19	38	2.13	0.03
	73	14 March	(12:38, 21:00)	(27, 59, 23)	1,203	(99, 149)	17	–	–	0.65
	74	15 March	(12:50, 21:00)	(29, 59, 23)	521	(86, 148)	13	1	0.03	1.18
	75	16 March	(12:45, 21:00)	(27, 59, 23)	323	(63, 102)	19	–	–	1.64
	76	17 March	(12:50, 21:00) ^a	(27, 58, 24)	2,194	(89, 129)	24	5	0.28	1.85
	77	18 March	(12:50, 21:00)	(25, 57, 25)	1,022	(71, 94)	13	–	–	1.81
	78	19 March	(12:40, 21:00)	(22, 56, 24)	50	(47, 83)	13	–	–	1.52
	79	20 March	(16:32, 21:00)	(54, 55, 24)	37	(45, 66)	21	–	–	1.04
	80	21 March	(12:45, 21:00)	(23, 54, 23)	465	(75, 105)	19	–	–	0.48
	81	22 March	(12:45, 21:00)	(21, 53, 23)	51	(68, 86)	14	–	–	–
	82	23 March	(13:33, 21:14)	(29, 52, 20)	59	(41, 77)	14	1	0.03	–
	83	24 March	(12:45, 21:00)	(19, 52, 23)	178	(79, 114)	21	–	–	–
	84	25 March	(12:00, 20:20) ^a	(10, 51, 30) ^b	3,032	(91, 156)	24	28	1.16	–
	85	26 March	(12:05, 20:19)	(10, 50, 30) ^b	888	(49, 74)	21	–	–	–
2022	29	29 January	(12:42, 21:00)	(39, 75, 31)	187	(32, 118)	31	–	–	–
	30	30 January	(12:42, 21:00)	(37, 75, 31)	29	(23, 59)	46	–	–	–
	31	31 January	(12:47, 21:00)	(37, 74, 32)	33	(42, 74)	19	–	–	–
	32	1 February	(12:51, 21:00)	(37, 74, 32)	45	(70, 120)	17	–	–	–
	33	2 February	(12:40, 21:00)	(34, 74, 33)	484	(88, 135)	16	–	–	0.42
	34	3 February ^c	(12:40, 21:00) ^a	(33, 74, 33)	2,168	(90, 217)	21	12	0.45	0.76
	35	4 February ^c	(12:40, 21:00)	(32, 73, 34)	393	(56, 112)	36	–	–	0.93
	36	5 February	(12:39, 21:00)	(31, 73, 34)	1,029	(83, 123)	16	–	–	0.92
	37	6 February	(12:40, 21:00)	(30, 72, 34)	32	(64, 109)	19	–	–	0.69
	39	8 February	(12:39, 21:00)	(28, 70, 34)	33	(74, 113)	18	–	–	–
	40	9 February	(12:46, 21:00)	(28, 69, 35)	34	(78, 101)	23	–	–	–
	41	10 February	(12:45, 21:00)	(29, 69, 35)	441	(63, 121)	30	–	–	–
	42	11 February	(12:45, 21:00)	(26, 68, 35)	196	(61, 87)	20	–	–	–
	43	12 February	(12:38, 21:00)	(25, 67, 36)	116	(46, 61)	20	–	–	–

Note. The columns indicate respectively the: (1) year; (2) day of the year (DOY); (3) calendar date; (4) time coverage; (5) characteristic elevation values (start of session, peak value, and end of session); (6) 99th percentile of the retrieved liquid water path along the slant direction; (7) range of retrieved zenith wet delay values; (8) 99th percentile of the wind speed measured by the TDCS meteo station; (9) 99th percentile of the instantaneous rain rate measured by the TDCS meteo station; (10) average rain rate during the pass (integral of the instantaneous rain rate divided by the pass duration); and (11) maximum pointing offset between the deep space antenna and the TDCS when in *Sun avoidance* mode.

^aReduced portions of these passes were analyzed due to the adverse weather conditions. Specifically, we removed all data when one of the following conditions was met: (i) rain was detected by the TDCS meteo station, (ii) the dew blower was active, and (iii) liquid water path along the slant direction was above 2,000 g/m². ^bData collected at elevations lower than 15° were removed during the data pre-processing. ^cThe Ka transponder lost the lock on the range in sporadic events, likely as a result of bad weather conditions at the station.

autumn in Malargüe. During these passes, the round-trip light time (RTLTL) ranged from 1,501 s at the beginning of March to 1,518 s at the end. At the same time, the maximum elevation ranged from 60° to 51°, with only a few passes going below 20°.

The remaining 14 passes are related to the second solar conjunction experiment (SCE2), which occurred between 29 January and 12 February 2022, corresponding to the local summer. Here, the RTLTL ranged from 1,471 s in

late January to 1,330 s in early February. The elevation was more favorable with respect to SCE1, with maximum values ranging from 75° to 67° and no pass going below 25°.

Both solar conjunctions are characterized by extremely low values of elongation, with local minima of 1.2° and 2.1° occurring on 17 March 2021 and 4 February 2022, respectively. For tracking passes characterized by elongation values smaller than 3° the so called *Sun avoidance* mode was used, which consists in applying an offset between the TDCS pointing direction and the one of the deep space antenna to avoid the intrusion of solar radiation in the TDCS beamwidth. The side effect of this procedure is the progressive divergence between the air volumes observed by the TDCS and by the deep space antenna as the pointing offset increases.

Among the atmospheric parameters shown in Table 1, the range of TDCS-retrieved zenith wet delay measurements provides an indication of the potential improvement that can be obtained when tropospheric calibrations are introduced in the orbit determination process.

Values of the TDCS-retrieved liquid water path (LWP) above ~10 g/m² indicate the presence of condensed water (clouds or fog) along the instrument line-of-sight. This quantity scales with the length of the propagation path through the cloud. Therefore, values of LWP > 500–1,000 g/m² (mapped to zenith), characteristic of thick cloud formations, may suggest the presence of rain within the sampled air volume. This information is complemented by the ground rain rate data measured close to the deep space antenna. Both these parameters are used for data quality assessment and to identify periods of adverse weather conditions for the TDCS calibrations. This is because the presence of clouds, rain, and horizontal atmospheric inhomogeneities along the slant-path can affect the accuracy of the retrieval algorithm, especially at low elevations.

Finally, the wind speed (WS) at ground level provides a twofold indication: on one side it indicates the strength of the vibrations induced on the TDCS mechanical structure, which represent an additional noise source for the calibrated data; on the other side, it represents a proxy for the presence of turbulent eddies in the lower portions of the atmosphere, which affect the accuracy of the TDCS calibrations (Lasagni Manghi et al., 2019).

4. Orbit Determination Analysis

4.1. Introduction

With the arrival in its final orbit scheduled for March 2026, the Mercury planetary orbiter (MPO) will perform the most precise radio science experiments ever conducted on Mercury. Before the orbital phase, the radio tracking system will be turned on, for experimental purposes, only concurrently with solar conjunctions to perform general relativity tests. A total of six SCE will be executed during the cruise phase: the presented work is based on the data collected during the first two conjunction experiments.

The analysis consists in performing side by side orbit determination processes using Doppler and ranging data collected during SCE1 and SCE2. The first orbit determination was performed applying GNSS-based tropospheric calibrations, while the second was performed applying TDCS calibrations. The dynamical and observational models, the data pre-processing procedures, and the filter setup were all maintained fixed between the two estimations in order to isolate the contribution of the tropospheric calibrations to the overall quality of the data.

4.2. Data Selection and Processing

The data set comprised X- and Ka-band Doppler and range observables, collected at ESA's deep space ground station in Malargüe, which were delivered in TTCP format (Ricart, 2018). A first processing step consisted in removing the delay introduced by the electronic systems and by the antenna optical system of the ground station, which are measured during dedicated calibration sessions before and after the tracking passes. The second step consisted in removing the delays introduced by the spacecraft, which are obtained as a combination of calibration test results performed on ground and auto-calibration test results performed onboard before each pass (provided by the spacecraft telemetry). These delays are among the largest contributors to the noise of the range measurements, so their accurate calibration is of key importance to reduce the a priori uncertainty of the range biases, which are estimated for each tracking pass.

Finally, the data was reduced by removing all measurements collected at elevation angles lower than 15° and by manually discarding the outliers through a visual inspection of the Doppler and range residuals at 1 s count time.

4.3. Media Calibrations

During periods of superior solar conjunction, the solar plasma becomes the highest contributor to the Doppler and range noises and is difficult to predict via analytical models due to short/medium scale variations of the electron density over the signal path (Verma et al., 2013). To mitigate the effect of the solar plasma and of the Earth's ionosphere, the MPO uses a particular communication technique, called multi-frequency link, in which radiometric measurements at X/X, X/Ka, and Ka/Ka bands are linearly combined to remove the dispersive signal components (Bertotti et al., 1993; Mariotti & Tortora, 2013). This can be seen by expressing the range and Doppler observables for a coherent two-way link as the sum of a non-dispersive component z_{nd} and of two components that scale with the uplink and downlink carrier frequencies, f_{\uparrow} and f_{\downarrow} :

$$z = z_{nd} + \frac{P_{\uparrow}}{f_{\uparrow}^2} + \frac{P_{\downarrow}}{f_{\downarrow}^2} \quad (1)$$

In this expression, the coefficients P_{\uparrow} and P_{\downarrow} are proportional to the total electron content of the medium (electrons/m²) for the range measurements and to its time derivative for the Doppler ones. Thanks to the multi-frequency link, three independent observables are acquired simultaneously by the ground station, namely z_{xx} , z_{xk} , and z_{kk} . By writing Equation 1 for each of the observables we obtain a system of three equations in the three unknowns P_{\uparrow} , P_{\downarrow} , and z_{nd} . Solving for the non-dispersive term, which represents the plasma-free observable used in the subsequent analysis, we obtain the following expression:

$$z_{nd} = \left(\frac{1}{\beta^2 - 1} \frac{\alpha_{xx}^2}{\alpha_{kk}^2} \frac{\alpha_{xk}^2 - \alpha_{kk}^2}{\alpha_{xx}^2 - \alpha_{xk}^2} \right) z_{xx} + \left(\frac{1}{\beta^2 - 1} \frac{\alpha_{xk}^2}{\alpha_{kk}^2} \frac{\alpha_{kk}^2 - \alpha_{xx}^2}{\alpha_{xx}^2 - \alpha_{xk}^2} \right) z_{xk} + \left(\frac{\beta^2}{\beta^2 - 1} \right) z_{kk} \quad (2)$$

where $\alpha_{kk} = \frac{3360}{3599}$, $\alpha_{xk} = \frac{3344}{749}$, and $\alpha_{xx} = \frac{880}{749}$ are the turnaround ratios, and $\beta = \frac{f_{\uparrow k}}{f_{\uparrow x}}$ is the ratio between the X- and Ka-band uplink frequencies. This method has been successfully applied in the past to the Cassini Doppler measurements at low elongations, showing a stability in the order of $1 - 2 \times 10^{-14}$ in terms of Allan deviation at 1,000 s intervals (Tortora et al., 2004). However, for impact parameters of few solar radii ($b \lesssim 7R_{\odot}$) the noise cancellation scheme failed due to the high density gradients in the corona (depending on the solar activity) and to possible signal losses at X-band.

Two types of tropospheric calibrations, whose main features are summarized in Table 2, were applied in separate orbit determination processes and compared in the following sections:

1. Standard tropospheric calibrations were generated by the ESOC Navigation Support Office (OPS-GN) according to the procedures described by Feltens et al. (2018), using the *FDmedCal* component of the *NAPEOS* v4.0 software. Specifically, OPS-GN routinely processes GNSS data as part of its activities for the International GNSS Service providing, among others, 48 hr time series of total zenith tropospheric delay with a 5 min time resolution. At the same time, pressure data collected by the deep space antenna weather station at a sampling interval of 2 s were used to retrieve the zenith hydrostatic delay (ZHD) using the model of Saastamoinen (1972). The hydrostatic delay was then scaled to the antenna reference height (i.e., the crossing point between elevation and azimuth axes) using the formulation by Estefan and Sovers (1994). The wet delay was simply obtained as the difference between the total delay and the hydrostatic component. Finally, wet and hydrostatic seasonal models for the Malarge site were subtracted from the delay time series, which were then fitted with degree 4 time-normalized polynomials of 6 hr intervals according to the control statement processing (CSP) format described by JPL (2008);

Table 2
Summary of Tropospheric Delay Calibration System and Global Navigation Satellite System-Based Calibrations Data Processing

Parameter	OPS-GN	TDCS
Time resolution (raw data)	2 s (ZHD) and 5 min (ZTD)	2 s (ZHD) and 2 s (ZWD)
Data reduction	Polynomial fit 6 hr intervals, degree 4	20 s compression
Software	NAPEOS v4.0 (<i>FDmedCal</i>)	RPG/UniBo
Mapping functions	Niell	None

2. TDCS calibrations were generated from sky brightness temperature measurements and concurrent meteorological data, according to the procedures described by Lasagni Manghi et al. (2021). A neural network retrieval algorithm, trained for the Malargüe site using ERA-Interim reanalysis data (ECMWF), was used to derive the slant wet delay along the spacecraft line of sight from the TDCS. The slant wet delay was then mapped to zenith using the Niell mapping function to comply with legacy orbit determination tools (the path is converted back to the boresight within the orbit determination tool, so no mapping is effectively applied) and scaled to the antenna height. Similarly to standard calibrations, the ZHD was derived from pressure measurements of the TDCS meteo station according to the model of Saastamoinen (1972) and scaled to the deep space antenna reference height. Both the wet and hydrostatic delays were compressed to 20 s time intervals and written to CSP format using a piecewise linear fit.

4.4. Dynamical Model

The gravitational accelerations considered for this analysis included relativistic point-mass gravity for the Sun, the Solar System planets, and their satellites. Higher order spherical harmonics were included for Mercury and the Sun. The gravitational coefficients and state vectors of the different bodies were taken from JPL's DE438 planetary ephemerides.

Concerning non-gravitational accelerations, the largest contribution is given by the solar radiation pressure, which was computed using a standard flat plates model and assuming a polyhedral shape for the main spacecraft components. Surface thermo-optical properties were considered to vary linearly between the launch and the end of mission.

Both of the analyzed SCE were characterized by the absence of thrusted maneuvers during the tracking intervals. Similarly, no reaction wheel desaturation maneuver was performed during the tracking intervals to preserve the coherency of the estimated spacecraft trajectories. Attitude data needed for the computation of the solar radiation pressure was retrieved from the operational SPICE kernel data set (ESA SPICE Service, 2022, <https://doi.org/10.5270/esa-dwuc9bs>).

4.5. Filter Setup

The orbit determination was performed using the mission analysis, operations and navigation toolkit environment (MONTE) software developed by NASA's Jet Propulsion Laboratory (Evans et al., 2018). This tool uses a weighted least-square batch filter, which minimizes the differences between the observed and the simulated measurements, also known as residuals, by adjusting the values of the dynamical and observational parameters shown in Table 3.

Specifically, *global* parameters are estimated once for the whole testbed campaign, while *local* parameters are estimated separately for each tracking pass. As a consequence, the estimated spacecraft trajectory is composed of separate trajectory arcs that can present discontinuities at the interval boundaries.

5. Results

After a careful calibration of the dispersive noise sources, using the multi-frequency link described above (Section 4.3), and of the of spacecraft and ground station delays, the processed radiometric measurements are

Table 3
Estimated Parameters and Their Corresponding a Priori Knowledge

Parameter	Type	N_{est}	<i>A priori</i> σ	<i>A priori value</i>
Spacecraft position	Local	$3 \cdot N_{arcs}$	100 km	ESA Spice kernels
Spacecraft velocity	Local	$3 \cdot N_{arcs}$	1 m/s	
Solar radiation pressure scale factor	Local	$1 \cdot N_{arcs}$	1	1
Ground station range bias	Local	$1 \cdot N_{arcs}$	1 km	0 km
S/C center of mass position (body frame)	Global	3	10 cm	(0, 0, 0) m

assumed to be mostly affected by mechanical noise from wind buffeting on the ground station antenna structure and by tropospheric errors.

When tropospheric calibrations are included within the orbit determination process, the radiometric measurements are affected by a variable amount of uncalibrated (or residual) tropospheric delay and by additional error sources, which are introduced by the calibrations.

For the TDCS these sources include intrinsic errors, such as the thermal noise of the microwave radiometer receivers or the losses of the optical components, and scene-dependent errors induced by the retrieval algorithm and by the mismatch between the air volumes within the beam of the deep space antenna and the beam of the TDCS antenna. Some of these individual contributions can be estimated through laboratory testing or simulations and were the subject of previous investigations by the authors (Graziani et al., 2014; Maschwitz et al., 2019). However, predicting the overall tropospheric error on 2-way radiometric measurements from the individual error contributions is a challenging task, since most of these error sources are mutually correlated and depend on atmospheric variables which can be difficult to assess, such as the amount of tropospheric turbulence contained in the antenna beam.

For the current analysis we opted for an end-to-end approach, which consists in directly evaluating the statistics of the Doppler and range residuals and comparing them to the system requirements. Due to the linearized nature of the orbit determination filter, any improvement in the measurement residuals is in fact directly proportional to the improvement in the accuracy of the estimated parameters, such as the rotational state and gravitational field of Mercury, or the parameterized post-Newtonian parameters of the general relativity (Buccino et al., 2021; Iess et al., 2018).

An initial assessment of the TDCS calibration quality is obtained by computing the root mean square (rms) value of the Doppler residuals at 60 s count time for each tracking pass and by comparing its value with the one obtained using standard GNSS calibrations. The count time value of 60 s was selected since it is sufficiently smaller than the characteristic time scales of the typically investigated processes and sufficiently large to avoid numerical noise issues (Zannoni & Tortora, 2013), thus representing a standard case for radioscience applications (Durante et al., 2019; Gomez Casajus et al., 2021; Tortora et al., 2016; Zannoni et al., 2020).

Similarly, the calibration quality on range measurements is evaluated by comparing the rms values of the residuals at sampling intervals of 1 s, corresponding to the interval provided in the input TTCP files (the real integration time coming from the ground station receiver configuration is 2 s). It should be noted that this approach is only useful to evaluate the random component of the tropospheric range error (i.e., the scintillation). Tropospheric delay biases, which typically represent the largest error contribution to range measurement, are difficult to quantify in a multi-arc orbit determination, being often absorbed by other estimated physical quantities such as the initial spacecraft state or the non-gravitational accelerations.

A further assessment of the TDCS calibration quality is obtained by computing the overlapping Allan standard deviation (ASD) of the Doppler residuals at 1 s count time and comparing its value at characteristic time scales with the ones obtained for standard GNSS calibrations.

In the following, the two SCE are treated separately to account for seasonal variations of the observing conditions (e.g., elevation profiles, air temperatures and water vapor content). A summary of the performances for the whole test campaign will then be given in Section 6.

5.1. First Solar Conjunction Experiment

Figure 1 depicts the Doppler residuals at 60 s count time for SCE1. A comparison of the rms values for both Doppler and range residuals of individual tracking passes is given in Table 4. An average Doppler noise reduction of 45% is observed when switching between the GNSS-based and TDCS calibrations, with only two passes showing reductions of less than 20% and a maximum reduction of 64% on 13 March.

Furthermore, the Doppler autocorrelation function is reduced for most of the tracking passes, as shown in Figure 2 for the test case of the 15 March pass, indicating a whitening of the residuals. For this test case, the Doppler autocorrelation is non-zero only for time delays <10 s and around the RTLTL, as a result of the two-way radio signal passing through the same air volume during both uplink and downlink. This pattern indicates the

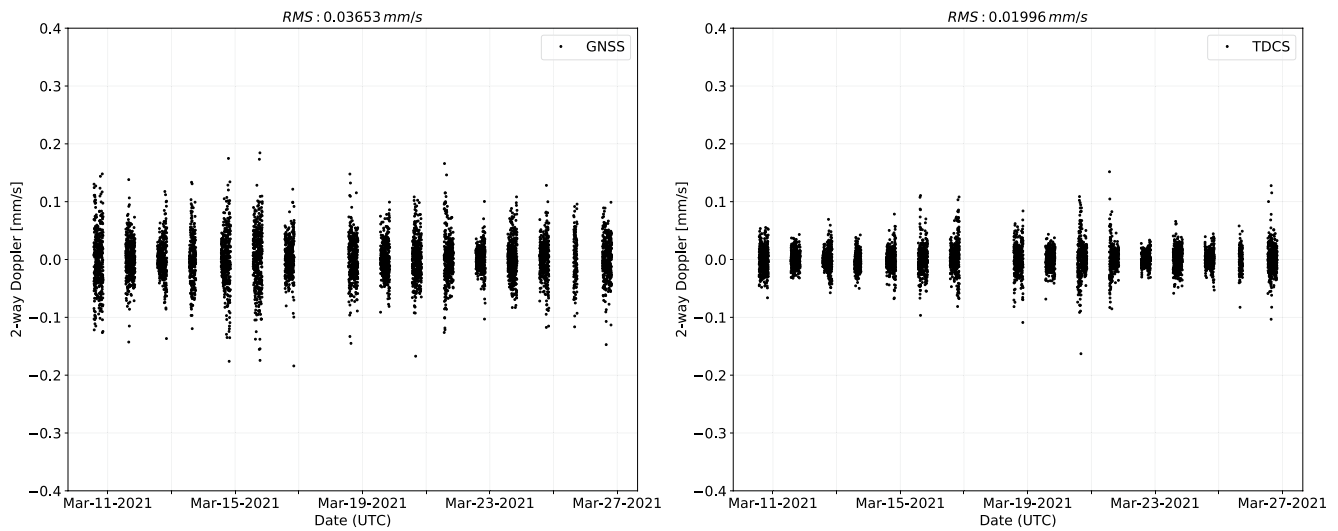


Figure 1. Comparison of the Doppler residuals at 60 s count time for the first solar conjunction experiment. Left: using global navigation satellite system-based calibrations; right: using tropospheric delay calibration system calibrations.

presence of either wind-induced mechanical noise from the ground station antenna structure or uncalibrated tropospheric errors at short time scales, which are likely due to spatial inhomogeneities caused by the offset and shape mismatch between the TDCS beam and the ground station antenna beam. These two effects are virtually undistinguishable since they have the same transfer function for two-way signals (Armstrong et al., 2008). A

Table 4
Rms Values of the Doppler and Range Residuals for Individual Tracking Passes of the First Solar Conjunction Experiment

DOY	Date	Rms of Doppler res. ($\mu\text{m/s}$) (full link, $T_C = 60$ s)			Rms of range res. (cm) (full link, $T_S = 1$ s, $T_{GS} = 2$ s)		
		GNSS	TDCS	Ratio	GNSS	TDCS	Ratio
69	10 March	49.91	20.59	0.41	4.31	4.27	0.99
70	11 March	33.30	12.98	0.39	2.97	2.98	1.00
71	12 March	29.97	16.94	0.57	2.99	2.99	1.00
72	13 March	41.44	15.05	0.36	3.05	3.03	0.99
73	14 March	44.67	17.21	0.39	3.17	3.09	0.97
74	15 March	50.98	22.90	0.45	3.29	2.94	0.89
75	16 March	31.05	25.85	0.83	3.15	3.16	1.00
77	18 March	35.40	23.32	0.66	3.08	3.07	1.00
78	19 March	28.28	15.44	0.55	2.93	2.89	0.98
79	20 March	35.79	30.01	0.84	2.88	2.91	1.01
80	21 March	38.01	22.28	0.59	2.87	2.85	0.99
81	22 March	20.21	10.92	0.54	2.89	2.87	0.99
82	23 March	32.63	18.16	0.56	2.91	2.88	0.99
83	24 March	31.44	13.34	0.42	2.89	2.88	0.99
84	25 March	39.89	19.35	0.49	2.91	2.90	0.99
85	26 March	32.84	23.44	0.71	2.91	2.85	0.98
Average		35.99	19.24	0.55	3.08	3.03	0.99
95th Percentile		50.18	26.89	0.83	3.54	3.43	1.01

Note. The Doppler count time is $T_C = 60$ s; the range sampling interval is $T_S = 1$ s, while the true ground station integration time is $T_{GS} = 2$ s.

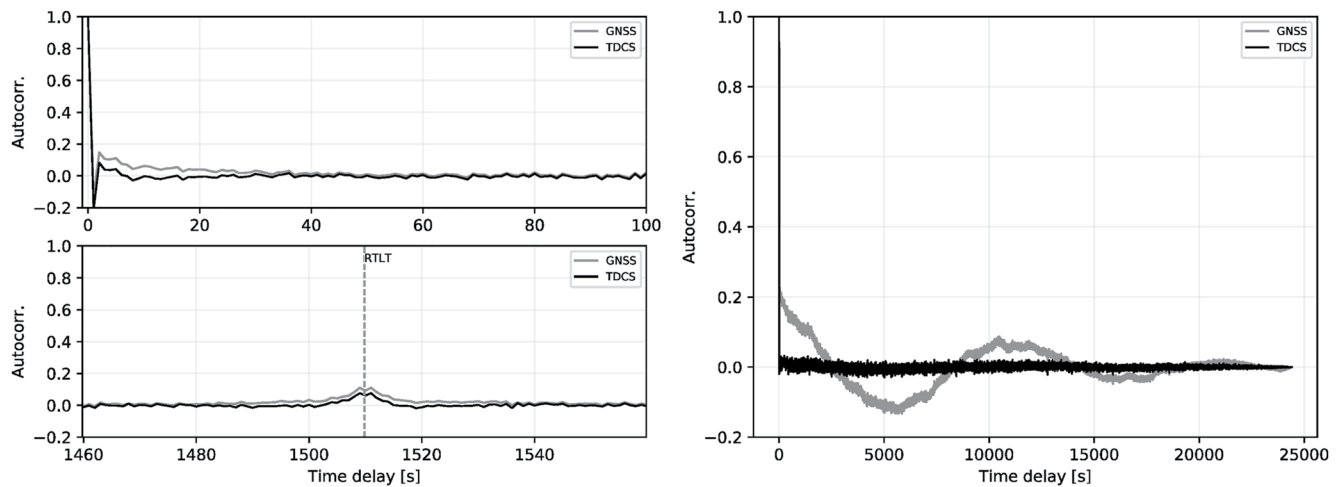


Figure 2. Autocorrelation of the residuals for the pass of 15 March. Left: Doppler residuals at 1 s count time. The upper plot shows a zoom at short time delays, while the lower plot shows a zoom around the round-trip light time (RTLT \approx 1,510 s, dashed line); right: range residuals.

small noise reduction of 1%, on average, is observed for the range residuals at 1 s integration times. At these time scales the range error is in fact dominated by other error sources (e.g., thermal noise) so the relative improvement from tropospheric calibrations is limited. However, a strong reduction is observed in the range autocorrelation function, indicating that most of the tropospheric-induced signatures in the residuals, which are not captured by the spatially averaged GNSS-based calibrations, are successfully removed by the TDCS, thus improving the robustness of the physical parameters estimated within the orbit determination process.

It should be noted that the data recorded on 17 March was removed from the analysis due to the presence of rain for the majority of the tracking interval. Similarly, portions of the data were removed from the tracking passes of 13 March and 25 March, when rain was detected by the TDCS meteo station or the antenna blower system was turned on (indicating the presence of residual water on the optical surfaces). This is because we expect a degrading quality of the retrieved delay in both situations.

Figure 3 depicts the Allan deviation of the Doppler residuals at 1 s count time for the individual tracking passes. The black dashed line represents the MORE requirement for 2-way Doppler residuals, corresponding to a maximum ASD value of $1.4 \cdot 10^{-14}$ at time intervals $\tau > 1,000$ s. This requirement was then mapped to shorter time intervals using the expression for white noise $ASD(\tau) = ASD(\tau_{req}) \sqrt{\tau_{req}/\tau}$, which is well approximating the behavior observed at typical time scales of interest for radioscience observations (e.g., 1–10,000 s). We can see that the stability requirement is satisfied for most of the tracking passes when using the TDCS calibrations, with the exception of the ones of 16 March and 20 March.

Finally, Figure 4 summarizes the ASD values for both scenarios at time intervals which are typical for radioscience applications, namely 20, 60, and 1,000 s. We can observe a consistent improvement for all tracking passes, with the highest reductions being obtained for longer time intervals. However, the stability improvement is less pronounced for the tracking passes characterized by low elongation values due to the pointing offset introduced by TDCS tracking system when the *Sun avoidance* mode was active.

5.2. Second Solar Conjunction Experiment

Figure 5 depicts the Doppler residuals at 60 s count time for SCE2. Rms values of both Doppler and range residuals for individual tracking passes are then compared in Table 5.

An average Doppler noise reduction of 58% is observed when switching from standard calibrations to TDCS calibrations, with no pass showing reductions of less than 41% and a maximum reduction of 73% on 3 February. An average noise reduction of 3% is instead observed for the range, with only two passes showing increased rms values.

This significant boost in the calibration performances with respect to SCE1 is likely the result of two contributing factors: on one hand, tracking passes recorded during SCE2 in summer can be characterized by higher turbulence

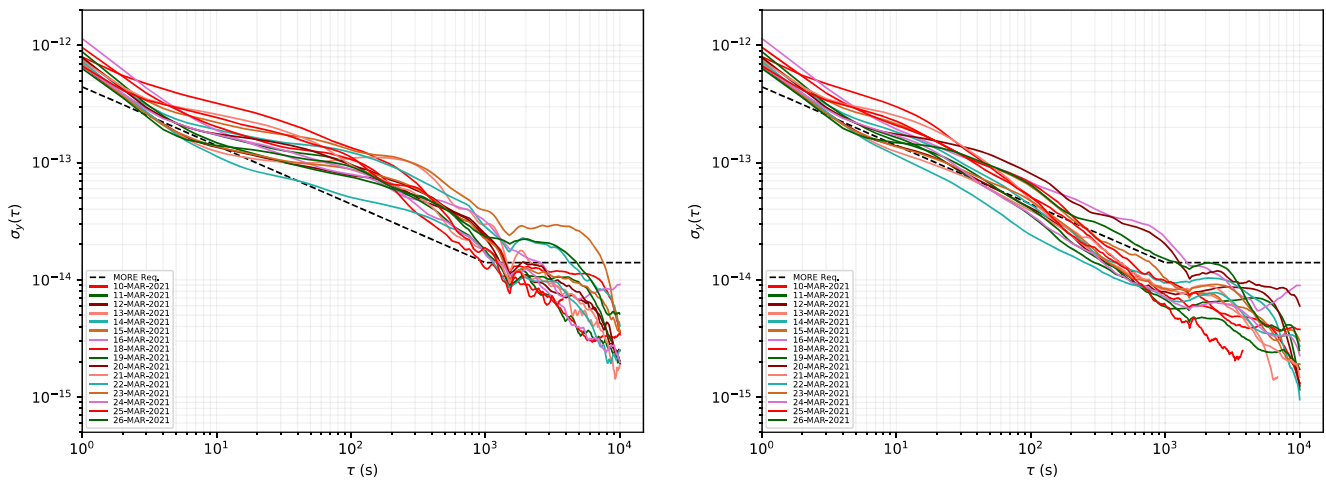


Figure 3. Allan deviation of the Doppler residuals at 1 s count time for the first solar conjunction experiment. Left: using global navigation satellite system-based calibrations; right: using tropospheric delay calibration system calibrations (2 s resolution, compressed to 20 s).

levels and water vapor content with respect to the ones recorded during SCE1 in autumn, as indicated by the increased noise values for the GNSS scenario; on the other hand, lower noise levels are observed in the TDCS scenario as a result of both hardware and software updates, which were implemented in the time interval between the two experiments, namely an improvement of the control procedures for the antenna tracking and the adoption of a shorter duty cycle for the internal gain calibration of the TDCS microwave radiometer.

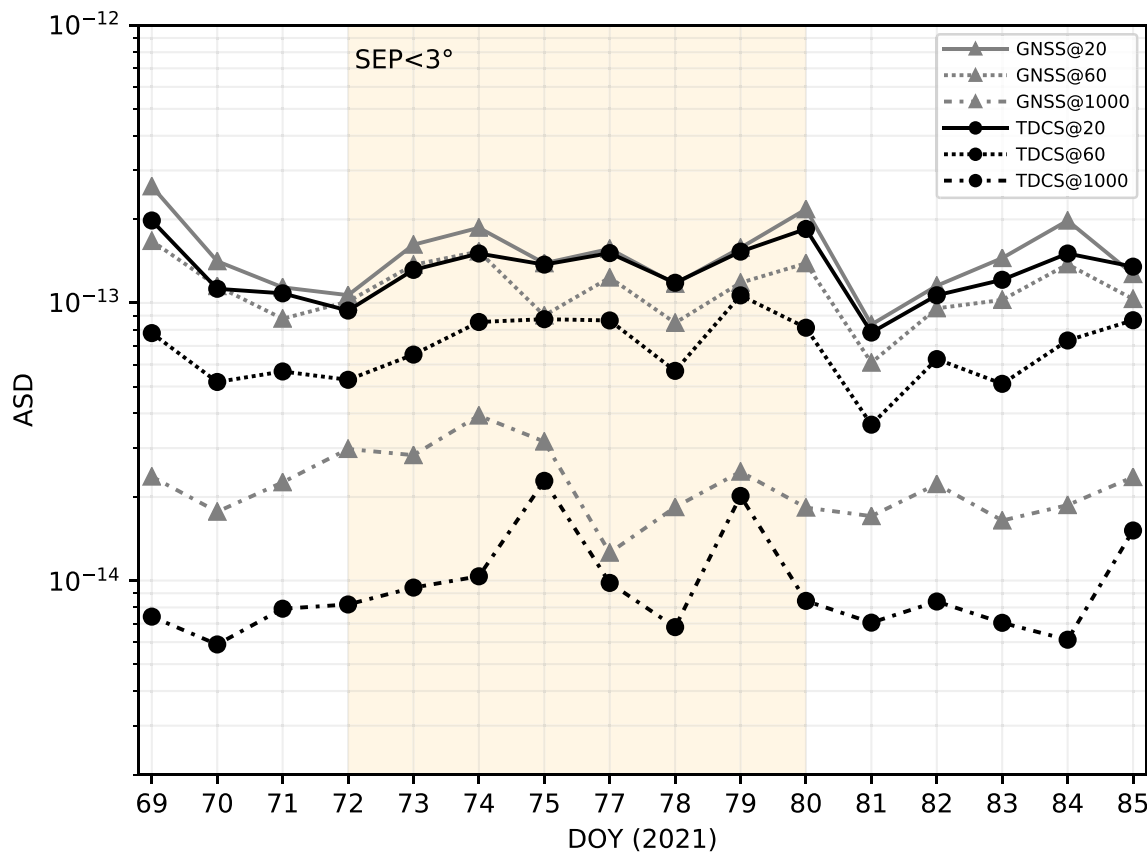


Figure 4. Comparison of the Allan standard deviation (ASD) values of the Doppler residuals at 1 s count time for the first solar conjunction experiment derived from global navigation satellite system (\blacktriangle) and tropospheric delay calibration system (\bullet) data; ASD values are displayed at characteristic stability intervals of 20 (solid line), 60 (dotted line), and 1,000 s (dash-dotted line). The shaded area marks the tracking passes for which the *Sun avoidance* mode is active (SEP angle $< 3^\circ$).

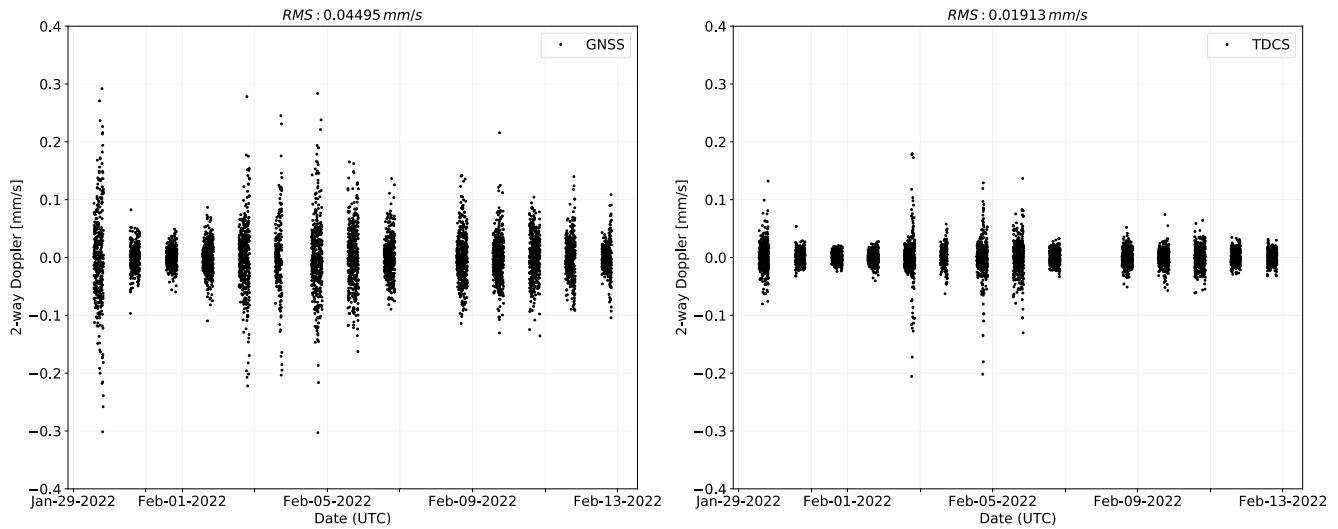


Figure 5. Comparison of the Doppler residuals at 60 s count time for the second solar conjunction experiment. Right: using global navigation satellite system-based calibrations; left: using tropospheric delay calibration system calibrations.

Figure 6 depicts the Allan deviation of the Doppler residuals at 1 s count time for the individual tracking passes of SCE2. As observed during SCE1, most of the tracking passes are consistent with the MORE requirements at stability intervals $\tau > 1,000$ s when TDCS calibrations are used, with the exception of 2 February. Most of the tracking passes also show a drop in the autocorrelation function for both Doppler and range residuals, as shown in Figure 7 for the test case of 29 January 2022, indicating a whitening of the residuals at timescales larger than 20 s. With respect to Figure 2, the higher autocorrelation observed at short timescales and around the RLTL

Table 5
Rms Values of the Doppler and Range Residuals for the Individual Tracking Passes of the Second Solar Conjunction Experiment

DOY	Date	Rms of Doppler res. ($\mu\text{m/s}$) (full link, $T_C = 60$ s)			Rms of range res. (cm) (full link, $T_S = 1$ s, $T_{GS} = 2$ s)		
		GNSS	TDCS	Ratio	GNSS	TDCS	Ratio
29	29 January	80.52	25.09	0.31	3.15	2.87	0.91
30	30 January	20.87	10.72	0.51	2.80	2.77	0.99
31	31 January	15.68	8.00	0.51	2.87	2.87	1.00
32	01 February	26.12	10.13	0.39	2.98	3.00	1.01
33	02 February	56.68	33.62	0.59	2.91	2.83	0.97
34	03 February	58.37	15.93	0.27	3.24	2.96	0.92
35	04 February	64.34	30.12	0.47	3.03	2.83	0.93
36	05 February	52.74	28.50	0.54	2.98	2.91	0.98
37	06 February	33.08	10.79	0.33	2.75	2.76	1.00
39	08 February	40.93	13.91	0.34	2.63	2.62	1.00
40	09 February	38.42	14.10	0.37	2.92	2.82	0.97
41	10 February	37.93	17.17	0.45	2.69	2.63	0.98
42	11 February	35.06	11.05	0.32	2.48	2.42	0.97
43	12 February	25.40	10.62	0.42	2.54	2.57	1.01
Average		41.87	17.12	0.42	2.85	2.78	0.97
95th Percentile		70.00	31.35	0.56	3.18	2.98	1.01

Note. The Doppler count time is $T_C = 60$ s; the range sampling interval is $T_S = 1$ s, while the true ground station integration time is $T_{GS} = 2$ s.

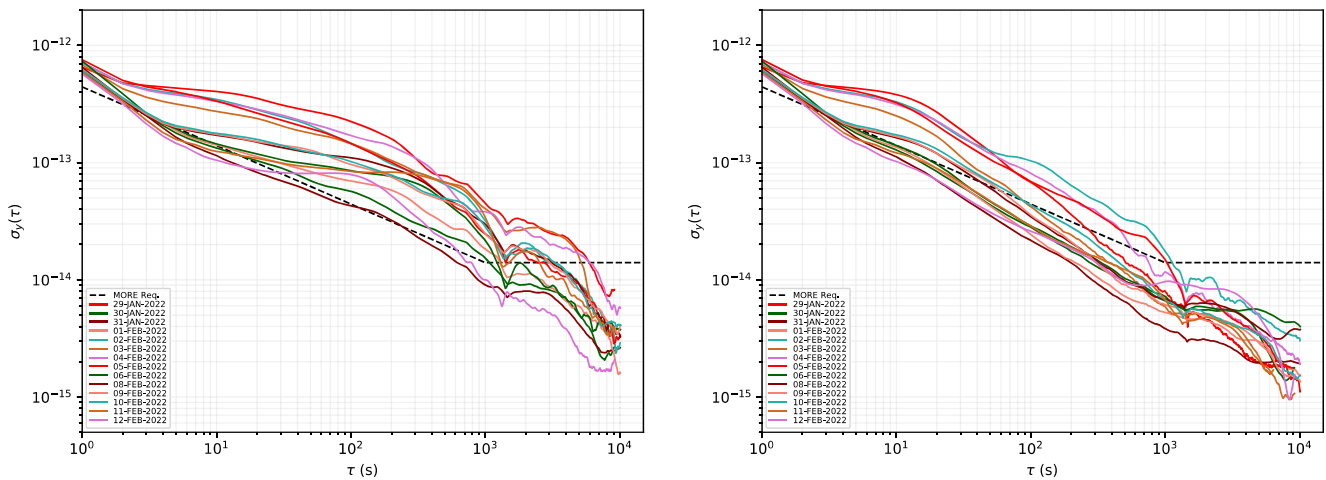


Figure 6. Allan deviation of the Doppler residuals at 1 s count time for the second solar conjunction experiment. Left: using global navigation satellite system-based calibrations; right: using tropospheric delay calibration system calibrations (2 s resolution, compressed to 20 s).

for SCE2 is likely due to a larger variability of water vapor and to higher wind speed at ground level, which increases the error contribution due to the beam offset.

Finally, Figure 8 summarizes the Allan deviation at characteristic stability intervals. With respect to the previous case, we observe a more pronounced reduction of the ASD curves at short stability intervals and particularly at 20 s, while the reduction is more or less consistent at 1,000 s. One noticeable exception is represented by the tracking pass of 12 February, where we observe a Doppler signature with characteristic timescales of a few hours, causing an increment in the ASD value at 1,000 s. The cause of this signature, which is introduced by the TDCS calibrations, is currently under investigation and is expected to be related to a retrieval algorithm error. It should also be mentioned that the stability reduction observed for tracking passes during which the *Sun avoidance* mode is active is less pronounced with respect to SCE1. This is likely due to higher elongation values, corresponding to lower pointing offsets, and higher elevation angles that reduce the volume mismatch between the TDCS and the deep space antenna beamwidths.

6. Conclusions

This work focused on the characterization of the TDCS performance during the scheduled tracking passes for the first two solar conjunctions experiments to be carried out by the BepiColombo mission. The analysis consisted

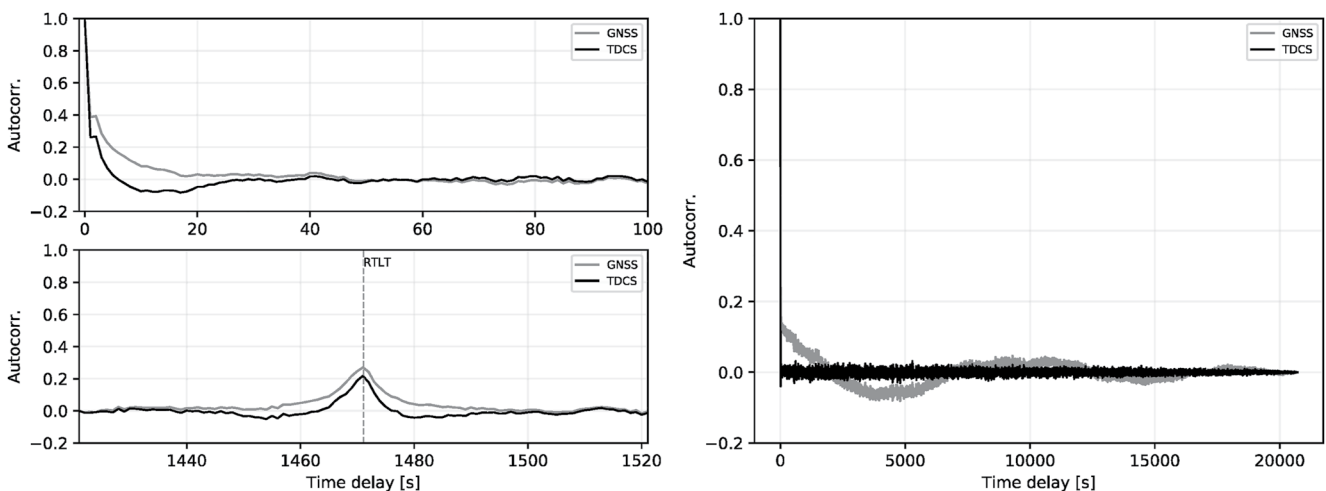


Figure 7. Autocorrelation of the residuals for the pass of 29 January 2022. Left: Doppler residuals at 1 s count time. The upper plot shows a zoom at short time delays, while the lower plot show a zoom around the round-trip light time (RTLT \approx 1,472 s, dashed line); right: range residuals.

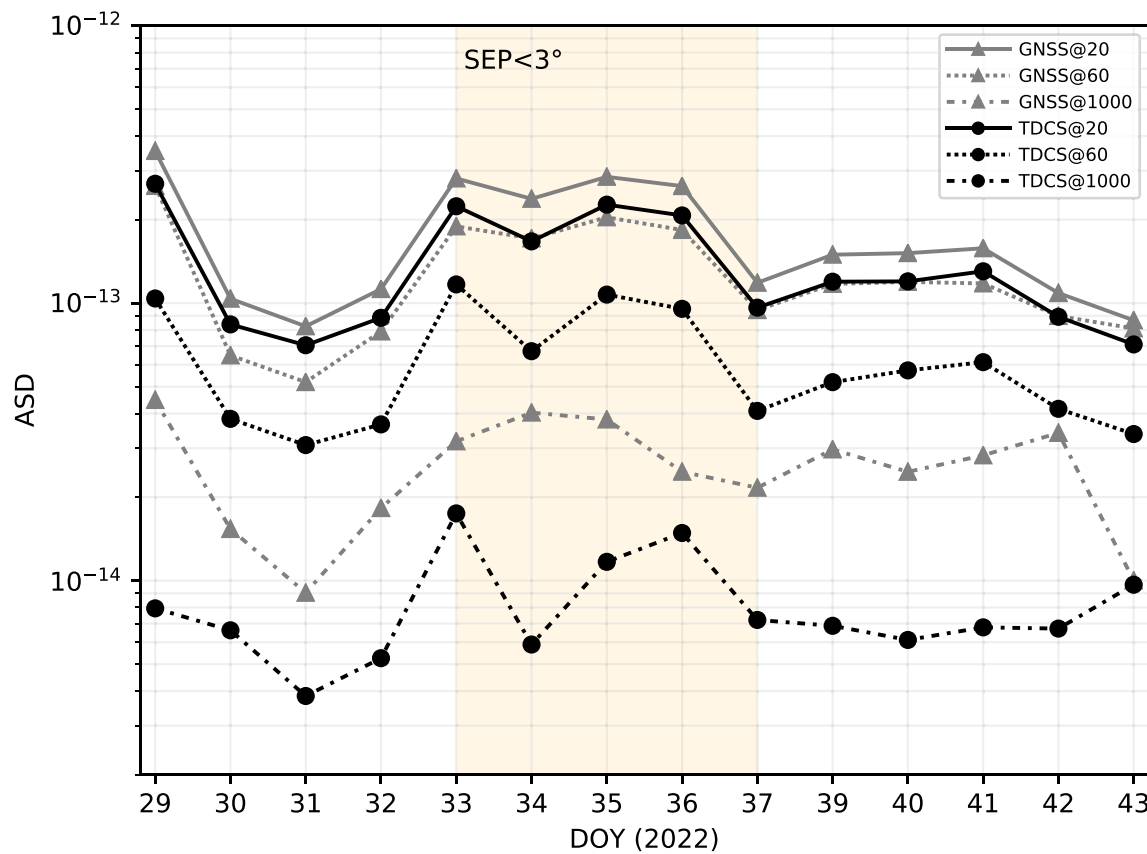


Figure 8. Comparison of the Allan standard deviation (ASD) values of the Doppler residuals at 1 s count time for the second solar conjunction experiment derived from global navigation satellite system (▲) and tropospheric delay calibration system (●) data; ASD values are displayed at characteristic stability intervals of 20 (solid line), 60 (dotted line), and 1,000 s (dash-dotted line). The shaded area marks the tracking passes for which the *Sun avoidance* mode is active (SEP angle $< 3^\circ$).

in a side-by-side comparison of Doppler and range residuals obtained when using alternatively GNSS-based or TDCS tropospheric calibrations as part of a multi-arc orbit determination process.

For the 16 tracking passes of SCE1, which occurred in March 2021 during the local autumn in Malargüe, we observed an average Doppler noise reduction of 45%, with a maximum reduction of 64%. The 14 tracking passes of SCE2, which occurred between January and February 2022 during the local summer, marked a significant boost with respect to SCE1, with an average Doppler noise reduction of 58% and a maximum reduction of 73%. Future investigations exploiting the TDCS calibrations will benefit from this noise reduction, with an improved accuracy of up to a factor of 3 for the estimated parameters of interest, namely the rotational state and gravitational field of Mercury or the general relativity post-Newtonian parameters. In addition to the accuracy improvement, the removal of non-white features in the residuals, which is observed from the reduction in the autocorrelation functions, corresponds to a reduction of the biases in the estimated parameters.

The results shown above are in line with the ones obtained for the Juno gravity science investigations, which report an average noise reduction of 46% with a maximum of 70%, when using the Advanced Water Vapor Radiometer (AWVR) installed at the DSS-25 ground station in Goldstone, California, in place of standard TSAC calibrations (Buccino et al., 2021). However, while the AWVR was specifically developed and built for the Cassini Gravity Wave Experiment, the TDCS core systems rely on commercial micro-wave radiometer technologies, such as RPG's Hatpro-G5, with significantly reduced upfront costs and improved flexibility of operations due to its smaller size.

A significant improvement was also observed in the Doppler stability at all characteristic time scales, when using TDCS calibrations. As a result, the MORE stability requirement for two-way Doppler observables, which is expressed in terms of Allan deviation at 1,000 s intervals, is satisfied for all but three tracking passes at extremely low elongation values, for which a deliberate pointing offset was applied to avoid solar intrusion in the TDCS beamwidth.

Overall, the performance exceeded the expectations based on the previous analysis for the orbit determination of Gaia, which was used as a qualification testbed. A contributing factor to these improved results is represented by an increased power and variability of the sky noise measured by the TDCS. Higher water vapor content and turbulence strength are in fact observed during daytime hours (as opposed to the nighttime observations of Gaia), and particularly during the summer months of SCE2. At the same time, the use of a Ka-band transponder and a multi-frequency link allowed for the complete cancellation of the dispersive noise sources from the Earth's ionosphere and the solar plasma. Finally, a series of hardware and software updates were implemented in the time interval between the two SCE, which further contributed to the reduction of the residual tropospheric noise after the calibrations.

It should be noted that some portions of the tracking passes, during which atmospheric conditions unfavorable for retrieval were observed (e.g., in case of heavy rain), were removed from the orbit determination analysis due to the degradation of the retrieval algorithm performance. The data set of tracking passes involving the TDCS is currently too small to produce a robust statistical characterization of the retrieval accuracy as a function of the possible atmospheric conditions, however the current data set shows that the use of TDCS permits a better calibration in particular during the local summer season when larger tropospheric turbulence and water vapor can occur. This is due to the capability of the TDCS to measure the delay introduced by the troposphere in the region illuminated by the deep space antenna beam with sampling rates higher than those of GNSS retrievals.

Future work will include additional observations from BepiColombo, Gaia, and other spacecraft routinely tracked from the Malargüe station, with the aim of producing an automatic filtering scheme for periods of low-quality data based on the observed atmospheric conditions.

Furthermore, a complete characterization of the range calibration performances (i.e., of the delay retrieval accuracy) will require switching from a multi-arc orbit determination approach to a single-arc approach with long propagation times, and evaluating the variations of the range biases estimated for each tracking pass. This effort will require implementing higher-fidelity dynamical models for the BepiColombo non gravitational accelerations, to maintain the trajectory coherence between successive tracking passes.

Data Availability Statement

Data sets of the MORE instrument have been downloaded from the ESA Planetary Science Archive (<http://archives.esac.esa.int/psa>) (Besse et al., 2018).

References

- Armstrong, J. W., Estabrook, F. B., Asmar, S. W., Iess, L., & Tortora, P. (2008). Reducing antenna mechanical noise in precision spacecraft tracking. *Radio Science*, 43(3), 1–7. <https://doi.org/10.1029/2007RS003766>
- Bertotti, B., Comoretto, G., & Iess, L. (1993). Doppler tracking of spacecraft with multi-frequency links. *Astronomy and Astrophysics*, 269, 608–616. Retrieved from <https://ui.adsabs.harvard.edu/abs/1993A&A.269.608B>
- Besse, S., Vallat, C., Barthelemy, M., Coia, D., Costa, M., De Marchi, G., et al. (2018). ESA's Planetary Science Archive: Preserve and present reliable scientific data sets. *Planetary and Space Science*, 150, 131–140. <https://doi.org/10.1016/j.pss.2017.07.013>
- Buccino, D. R., Kahan, D. S., Parisi, M., Paik, M., Barbinis, E., Yang, O., et al. (2021). Performance of Earth troposphere calibration measurements with the advanced water vapor radiometer for the Juno Gravity science investigation. *Radio Science*, 56(12), e2021RS007387. <https://doi.org/10.1029/2021RS007387>
- Cappuccio, P., Notaro, V., di Ruscio, A., Iess, L., Genova, A., Durante, D., et al. (2020). Report on first inflight data of BepiColombo's Mercury orbiter radio science experiment. *IEEE Transactions on Aerospace and Electronic Systems*, 56(6), 4984–4988. <https://doi.org/10.1109/TAES.2020.3008577>
- di Stefano, I., Cappuccio, P., & Iess, L. (2021). The BepiColombo solar conjunction experiments revisited. *Classical and Quantum Gravity*, 38(5), 055002. <https://doi.org/10.1088/1361-6382/abd301>
- Durante, D., Hemingway, D. J., Racioppa, P., Iess, L., & Stevenson, D. J. (2019). Titan's gravity field and interior structure after Cassini. *Icarus*, 326, 123–132. <https://doi.org/10.1016/j.icarus.2019.03.003>
- ESA SPICE Service. (2022). BepiColombo operational SPICE kernel dataset. <https://doi.org/10.5270/esa-dwuc9bs>
- Estefan, J., & Sovers, O. (1994). A comparative survey of current and proposed tropospheric refraction-delay models for DSN radio metric data calibration.
- Evans, S., Taber, W., Drain, T., Smith, J., Wu, H.-C., Guevara, M., et al. (2018). MONTE: The next generation of mission design and navigation software. *CEAS Space Journal*, 10(1), 79–86. <https://doi.org/10.1007/s12567-017-0171-7>
- Feltens, J., Bellei, G., Springer, T., Kints, M. V., Zandbergen, R., Budnik, F., & Schönemann, E. (2018). Tropospheric and ionospheric media calibrations based on global navigation satellite system observation data. *Journal of Space Weather and Space Climate*, 8, A30. <https://doi.org/10.1051/swsc/2018016>
- Gomez Casajus, L., Zannoni, M., Modenini, D., Tortora, P., Nimmo, F., Van Hoolst, T., et al. (2021). Updated Europa gravity field and interior structure from a reanalysis of Galileo tracking data. *Icarus*, 358, 114187. <https://doi.org/10.1016/j.icarus.2020.114187>

Acknowledgments

R. Lasagni Manghi, D. Bernacchia, M. Zannoni, L. Gomez Casajus, and P. Tortora are grateful to the Italian Space Agency (ASI) for financial support through the Agreement No. 2022-16-HH.0 for ESA's BepiColombo and NASA's Juno radio science experiments. The authors wish to acknowledge Caltech and the Jet Propulsion Laboratory for granting the University of Bologna a license to an executable version of the MONTE project edition software. The research described in this paper was carried out in the framework of ESA Contract 4000116932/16/NL/AF "Development of a Ground Tropospheric Media Calibration System for Accurate Ranging of Space Science Missions". Open Access Funding provided by Università degli Studi di Bologna within the CRUI-CARE Agreement.

- Graziani, A., Jarlemark, P., Elgered, G., Martellucci, A., Micolino, M., & Tortora, P. (2014). Assessment of ground-based microwave radiometry for calibration of atmospheric variability in spacecraft tracking. *IEEE Transactions on Antennas and Propagation*, 62(5), 2634–2641. <https://doi.org/10.1109/TAP.2014.2307582>
- Iess, L., Asmar, S., & Tortora, P. (2009). MORE: An advanced tracking experiment for the exploration of Mercury with the mission BepiColombo. *Acta Astronautica*, 65(5–6), 666–675. <https://doi.org/10.1016/j.actaastro.2009.01.049>
- Iess, L., Asmar, S. W., Cappuccio, P., Cascioli, G., De Marchi, F., di Stefano, I., et al. (2021). Gravity, geodesy and fundamental physics with BepiColombo's MORE investigation. *Space Science Reviews*, 217(1), 21. <https://doi.org/10.1007/s11214-021-00800-3>
- Iess, L., Budnik, F., Colamarino, C., Corbelli, A., Di Benedetto, M., Fabbri, V., et al. (2012). ASTRA: Interdisciplinary study on enhancement of the end-to-end accuracy for spacecraft tracking techniques. In *Proceedings of the International Astronautical Congress, IAC*, (pp. 53425–53435).
- Iess, L., Folkner, W., Durante, D., Parisi, M., Kaspi, Y., Galanti, E., et al. (2018). Measurement of Jupiter's asymmetric gravity field. *Nature*, 555(7695), 220–222. <https://doi.org/10.1038/nature25776>
- JPL. (2008). TRK-2-23 media calibration interface. 820-013. Deep Space Network (DSN), External Interface Specification, JPL D-16765, Revision C (draft). Retrieved from http://dawndata.igpp.ucla.edu/download.jsp?file=documents/Gravity/DATA_SET_DESCRIPTION/TRK-2-23_REVC_L5.PDF
- Lasagni Manghi, R., Maschwitz, G., Tirtira, P., Rose, T., Martellucci, A., De Vicente, J., et al. (2019). Tropospheric delay calibration system (TDCS): Design and performances of a new generation of microwave radiometers for ESA deep space ground stations. In *TT&C workshop*.
- Lasagni Manghi, R., Zannoni, M., Tortora, P., Martellucci, A., De Vicente, J., Villalvilla, J., et al. (2021). Performance characterization of ESA's tropospheric delay calibration system for advanced radio science experiments. *Radio Science*, 56(10), 1–14. <https://doi.org/10.1029/2021RS007330>
- Mariotti, G., & Tortora, P. (2013). Experimental validation of a dual uplink multifrequency dispersive noise calibration scheme for deep space tracking: Dual uplink incomplete link. *Radio Science*, 48(2), 111–117. <https://doi.org/10.1002/rds.20024>
- Maschwitz, G., Czekala, H., Orlandi, E., & Rose, T. (2019). Accuracy and performance of atmospheric delay by a RPG microwave radiometer with respect to ground calibration systems for ESA radio science. In *TT&C workshop*.
- Ricart, M. (2018). TTCP software interface control document (ICD) for RM datasets. (Issue 2.1).
- Saastamoinen, J. (1972). Atmospheric correction for the troposphere and stratosphere in radio ranging satellites. In S. W. Henriksen, A. Mancini, & B. H. Chovitz (Eds.), *The use of artificial satellites for geodesy*. <https://doi.org/10.1029/GM015p0247>
- Serra, D., Lari, G., Tommei, G., Durante, D., Gomez Casajus, L., Notaro, V., et al. (2019). A solution of Jupiter's gravitational field from Juno data with the orbit14 software. *Monthly Notices of the Royal Astronomical Society*, 490(1), 766–772. <https://doi.org/10.1093/mnras/stz2657>
- Tortora, P., Iess, L., Bordi, J. J., Ekelund, J. E., & Roth, D. C. (2004). Precise Cassini navigation during solar conjunctions through multifrequency plasma calibrations. *Journal of Guidance, Control, and Dynamics*, 27(2), 251–257. <https://doi.org/10.2514/1.997>
- Tortora, P., Zannoni, M., Hemingway, D., Nimmo, F., Jacobson, R. A., Iess, L., & Parisi, M. (2016). Rhea gravity field and interior modeling from Cassini data analysis. *Icarus*, 264, 264–273. <https://doi.org/10.1016/j.icarus.2015.09.022>
- Verma, A. K., Fienga, A., Laskar, J., Issautier, K., Manche, H., & Gastineau, M. (2013). Electron density distribution and solar plasma correction of radio signals using MGS, MEX, and VEX spacecraft navigation data and its application to planetary ephemerides. *Astronomy and Astrophysics*, 550, A124. <https://doi.org/10.1051/0004-6361/201219883>
- Zannoni, M., Hemingway, D., Gomez Casajus, L., & Tortora, P. (2020). The gravity field and interior structure of Dione. *Icarus*, 345, 113713. <https://doi.org/10.1016/j.icarus.2020.113713>
- Zannoni, M., & Tortora, P. (2013). Numerical error in interplanetary orbit determination software. *Journal of Guidance, Control, and Dynamics*, 36(4), 1008–1018. <https://doi.org/10.2514/1.59294>